Acta Biomaterialia 146 (2022) 145–158

Contents lists available at ScienceDirect

Acta Biomaterialia

journal homepage: www.elsevier.com/locate/actbio

Full length article

# Robust gelatin hydrogels for local sustained release of bupivacaine following spinal surgery

Jasper G. Steverink[a,b,c], Floris R. van Tol[a,c], Bas J. Oosterman[c], Tina Vermonden[e], Jorrit-Jan Verlaan[a,c], Jos Malda[a,b,d], Susanna Piluso[a,b,c,*]

[a] Department of Orthopaedics, University Medical Center Utrecht, Heidelberglaan 100, 3584CX Utrecht, the Netherlands
[b] Regenerative Medicine Utrecht, Utrecht University, Uppsalalaan 8, 3584CT Utrecht, the Netherlands
[c] SentryX B.V., Woudenbergseweg 41, 3711 AA Austerlitz, the Netherlands
[d] Department of Clinical Sciences, Faculty of Veterinary Medicine, Utrecht University, Yalelaan 1, 3584CL Utrecht, the Netherlands
[e] Department of Pharmaceutics, Utrecht Institute for Pharmaceutical Sciences (UIPS), Science for Life, Utrecht University, Universiteitsweg 99, 3508 TB, Utrecht, the Netherlands

ARTICLE INFO

*Article history:*
Received 9 December 2021
Revised 21 April 2022
Accepted 5 May 2022
Available online 11 May 2022

*Keywords:*
Gelatin
Local anesthetics
Cyclodextrin
Photo-crosslinking
Orthopedic implantation
Riboflavin

ABSTRACT

Adequate treatment of pain arising from spinal surgery is a major clinical challenge. Opioids are the mainstay of current treatment methods, but the frequency and severity of their side effects display a clear need for opioid-free analgesia. Local anesthetics have been encapsulated into sustained-release drug delivery systems to provide postoperative pain relief. However, these formulations are limited by rapid diffusion out of the surgical site. To overcome this limitation, we synthesized ring-shaped hydrogels incorporating bupivacaine, designed to be co-implanted with pedicle screws during spinal surgery. Hydrogels were prepared by riboflavin-mediated crosslinking of gelatin functionalized with tyramine moieties. Additionally, oxidized $\beta$-cyclodextrin was introduced into the hydrogel formulation to form dynamic bonds with tyramine functionalities, which enables self-healing behavior and resistance to shear. Feasibility of hydrogel implantation combined with pedicle screws was qualitatively assessed in cadaveric sheep as a model for instrumented spinal surgery. The *in-situ* crystallization of bupivacaine within the hydrogel matrix provided a moderate burst decrease and sustained release that exceeded 72 hours *in vitro*. The use of bupivacaine crystals decreased drug-induced cytotoxicity *in vitro* compared to bupivacaine HCl. Thus, the presented robust hydrogel formulation provides promising properties to enable the stationary release of non-opioid analgesics following spinal surgery.

**Statement of significance**

Currently, postoperative pain following spinal surgery is mainly treated with opioids. However, the use of opioids is associated with several side effects including addiction. Here we developed robust and cytocompatible gelatin hydrogels, prepared via riboflavin-mediated photocrosslinking, that can withstand orthopedic implantation. The implantability was confirmed in cadaveric instrumented spinal surgery. Further, hydrogels were loaded with bupivacaine crystals to provide sustained release beyond 72 hours *in vitro*. The use of crystallized bupivacaine decreased cytotoxicity compared to bupivacaine HCl. The present formulation can aid in enabling opioid-free analgesia following instrumented spinal surgery.



## 1. Introduction

Spinal surgery ranks amongst the most painful interventions overall, and adequate analgesic treatment remains a major clinical challenge [1,2]. Systemic medications, such as opioids, fulfil a central role in the treatment of postoperative pain following spinal surgery, but come at the cost of significant side effects, such as constipation, drowsiness and respiratory depression [3,4]. Further-

* Corresponding author at: Woudenbergseweg 41, 3711 AA Austerlitz, the Netherlands.
*E-mail addresses:* s.piluso-2@umcutrecht.nl, susanna.piluso@sentryx.nl (S. Piluso).

https://doi.org/10.1016/j.actbio.2022.05.007

more, the use of opioids is associated with the risk of development of opioid dependence or addiction [5,6]. Despite opioid use, high pain scores and inadequate postoperative pain relief are reported in the majority of patients [2,7,8]. The delicate balance between opioid efficacy and side effects displays a clear unmet need for alternative, opioid-free analgesics.

As postoperative pain is a local problem, specifically targeting the surgical site would eliminate most of the side effects of systemically administered analgesics. Local anesthetics (LA), such as lidocaine and bupivacaine, are well-suited to combat local pain, but are hampered by a short duration of action [9,10]. To overcome this limitation, various delivery systems for local anesthetics have been developed [10]. These systems involve mainly the delivery of local anesthetics via microparticles, liposomes and injectable polymer solutions [11]. For example, the incorporation of bupivacaine into polymeric microparticles based on poly (lactic-*co*-glycolic acid) (PLGA) improved the duration of action in comparison to bupivacaine solutions [12]. Similarly, encapsulation of local anesthetics into liposomes resulted in slow drug release and prolonged duration of the anesthetic effect [13]. Further, preclinical studies confirmed the improvement of bupivacaine safety profile after encapsulation into liposomes [14]. Recently, the incorporation of bupivacaine with meloxicam into a Biochronomer® polymer reduced postoperative pain for 72 hours [15]. Similar results were obtained when using a resorbable bupivacaine-impregnated collagen matrix (Xaracoll, Innocoll Pharmaceuticals) for the management of postoperative pain [16]. The use of these delivery systems can greatly improve the efficacy and duration of bupivacaine. However, all formulations are limited by a high initial burst release and rapid diffusion from the surgical site, thus giving limited analgesic effect beyond 24 hours [15,17–19]. Further, some formulations have degradation times well beyond the window of drug release leading to particle debris present at the injection site for weeks [20,21]. Moreover, increased myotoxicity of bupivacaine when combined with polymeric microparticles compared to 0.5% bupivacaine HCl solution has been reported [20].

Hydrogels provide a unique approach for the delivery of LA at specific sites, with improved efficacy and potential to reduce systemic toxicity. Indeed, they generally exhibit excellent tissue compatibility and tunable drug release profile, mechanical properties and degradation rate [22,23]. Surgical interventions provide an opportunity for administration of hydrogels by implantation, mitigating the need for injectability of the hydrogel formulation. For optimal performance in patients undergoing spinal surgery, a hydrogel that can simultaneously withstand high compression and shear forces during implantation is needed (Fig. 1A). To this end, we developed a hydrogel formulation for sustained release of bupivacaine based on a dual crosslinked hydrogel, that enables rapid recovery from repeated applications of high strain and shear. The proposed hydrogel system consists mainly of gelatin-tyramine, gelatin functionalized with tyramine moieties (GTA) [24]. Gelatin was selected as it is a natural polymer obtained by hydrolysis of collagen, and gelatin hydrogels have been used frequently in drug delivery as they are well-tolerated in various tissues [25,26]. Further, gelatin contains carboxylic and amino groups that can be used for its functionalization. Its molecular structure and specific amino acid sequence make it susceptible to enzymatic degradation, ensuring rapid clearance from the surgical site [27]. In this study, hydrogels were prepared by combining GTA with oxidized $\beta$-cyclodextrin (oB-CD) and photo-crosslinked using riboflavin (RB, vitamin B2)/ sodium persulfate (SPS), and exposure to visible light (Fig. 1B) [28]. The riboflavin/SPS photoinitiating system crosslinks two tyramine moieties into di-tyramine adducts. Furthermore, tyramine moieties can form inclusion complexes through interaction with the hydrophobic cavity of $\beta$-cyclodextrin, whilst oxidized groups on beta-cyclodextrin allowed for the coupling to amine groups on gelatin *via* imine bond formation [29–31].

Cyclodextrins ($\alpha$-, $\beta$- and $\gamma$-) are cone-shaped molecules extensively used in drug delivery, with $\beta$-cyclodextrin being the most often used [10]. Their main advantage is the capability to encapsulate drugs in the hydrophobic interior, while the hydrophilic exterior ensures water-solubility [32,33]. This inclusion complex formation can lead to increased solubility, and prolonged release of hydrophobic drugs [24,34]. In a hydrogel, cyclodextrins can also provide a means to achieve dynamic crosslinks *via* interactions with suitable moieties on a polymer backbone. Next to self-healing behavior, the inclusion complexes allow for dissipation of energy and thus enhance the mechanical properties of the hydrogel [31].

Here, we designed a hydrogel to be co-implanted with pedicle screws during instrumented spinal surgery. We hypothesized that these combined crosslink methods could provide the hydrogel with mechanical properties that ensure adequate resistance to the orthopedic implantation procedure, while the biodegradable hydrogel precursor could lead to swift degradation and removal from the surgical site [34,35]. We first evaluated the physical and mechanical properties of the designed hydrogel system.

Next, we investigated whether the proposed hydrogel system could act as a cytocompatible sustained-release formulation for local delivery of bupivacaine following spinal surgery.

## 2. Material and methods

### 2.1. Synthesis of gelatin-tyramine

Gelatin-tyramine (GTA) was synthesized as previously reported [24]. Briefly, gelatin (type A, porcine skin, Sigma-Aldrich) was dissolved in 2-(*N*-morpholino)ethanesulfonic acid buffer (MES, Sigma-Aldrich, 50 mM, pH 4.75) at a concentration of 1.67 wt.% and reacted with tyramine HCl (Sigma-Aldrich) in a 4:1 ratio of [Tyramine]:[COOH]. The reaction was performed in presence of 1-ethyl-3-(3-dimethylaminopropyl)carbodiimide hydrochloride (EDC, Sigma-Aldrich) and *N*-hydroxysuccinimide (NHS, Sigma-Aldrich) in a 2:1 ratio at 45 °C overnight. The reaction mixture was then dialyzed (MWCO 14 kDa cellulose dialysis membrane, Sigma-Aldrich) against deionized water for 72 hours and subsequently lyophilized. Yield of the reaction following dialysis and freeze drying was 77.3% (±6.9%).

The degree of functionalization (DoF) was determined by measuring the absorbance at 275 nm of 0.1 wt.% gelatin and GTA solutions. Absorbance was interpolated on a tyramine HCl standard curve and corrected for the absorbance of non-functionalized gelatin. The degree of functionalization was expressed as a percentage of the available COOH groups in gelatin (79 mmol/ 100 g) [36].

### 2.2. Synthesis of oxidized $\beta$-cyclodextrin (oB-CD)

$\beta$-cyclodextrin (B-CD, Sigma-Aldrich) was oxidized by modifying a previously described procedure [24]. B-CD was suspended in MilliQ-water followed by addition of sodium periodate ($NaIO_4$, Sigma-Aldrich) in [$NaIO_4$]:[B-CD] molar ratios up to 4:1, and stirred at room temperature. Aliquots of the reaction mixture were taken at predetermined time points to assess the degree of oxidation as a function of time. The reaction was quenched by adding glycerol in a 1:1 molar ratio with sodium periodate. The solution was then dialyzed (MWCO 0.5 kDa, VWR) against MilliQ-water in the dark at room temperature for 48 hours. Water was replaced six times daily. The purified solution was then lyophilized to obtain oxidized $\beta$-cyclodextrin (oB-CD). Proton Nuclear Magnetic Resonance ($^1$H NMR) in DMSO-d6 was used to confirm presence of aldehyde

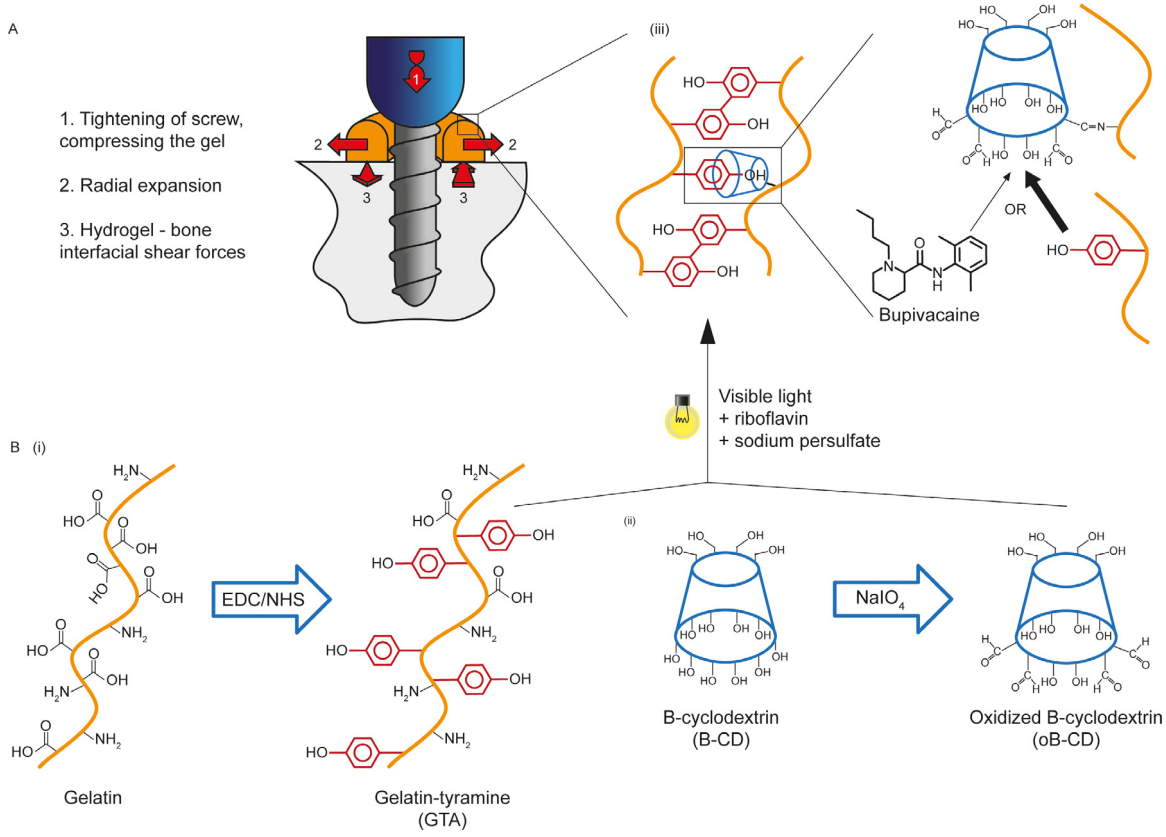


**Fig. 1.** Schematic illustration of hydrogel preparation and implantation. **A** Scheme of forces acting on the hydrogel during co-implantation with a pedicle screw. **B** (i) Functionalization of gelatin carboxyl groups with tyramine moieties via EDC/NHS mediated coupling and amide bond formation; (ii) oxidation of B-CD secondary hydroxyl groups to aldehyde groups in presence of sodium periodate ($NaIO_4$). For the sake of clarity only few of the primary and secondary hydroxyl groups of B-CD are shown in the schematic; (iii) hydrogel formation achieved by mixing GTA with oB-CD, in presence of riboflavin and sodium persulfate and exposure to visible light with Schiff-base formation between oB-CD and amine groups present on GTA and tyramine-tyramine photo-crosslinking. The cyclodextrin cavity can form inclusion complexes with both tyramine (high affinity, thick arrow) and bupivacaine (low affinity, thin arrow).

groups and quantify the oxidation degree as previously described [30]. Yield following dialysis and freeze drying was 55.8% (±5.2%).

### 2.3. Affinity assay by $^1H$ NMR of bupivacaine and tyramine for B-CD

To assess affinity of bupivacaine for the cavity of B-CD, a double reciprocal Benesi-Hildebrand plot was constructed using increasing concentrations of bupivacaine (1-8 mM) or tyramine (1-10 mM) in $D_2O$ (Sigma-Aldrich), while the B-CD concentration was kept constant at 11 mM. Samples were analyzed using $^1$H-NMR (400 mHz, Bruker, Leiderdorp, NL) and an association constant ($K_a$) was calculated [37,38]. $\Delta\delta_{max}$ was calculated as (1/intercept), after which the $K_a$ was calculated as (1/(slope*$\Delta\delta_{max}$).

### 2.4. Preparation of GTA hydrogels

Stock solutions of GTA, oB-CD, riboflavin 5'-monophosphate sodium salt (RB, Sigma-Aldrich) and sodium persulfate (SPS, Sigma-Aldrich) in deionized water were freshly prepared. Hydrogels were then formed by casting a pre-gel solution of various composition in cylindrical (8 mm diameter x 2 mm height) or ring-shaped (internal diameter 6 mm, external diameter 18 mm, height 6 mm) molds and exposed to visible light (400-700 nm) for 30 minutes. Light intensity at mold level was 60 mW/cm$^2$. Hydrogels were hydrated during the photo-crosslinking process to account for evaporation due to heat generated from the lamp. Following crosslinking, gels were washed in excess PBS to remove any unreacted reagents.

### 2.5. Sol fraction and equilibrium swelling of GTA hydrogels

After synthesis, hydrogels were dried in an oven at 37 °C ($m_{d1}$) and then incubated in phosphate-buffered saline (PBS, pH 7.4) at 37 °C until equilibrium swelling. After 24 hours, the swollen weight was recorded ($m_s$) and the gels were again dried ($m_{d2}$). Swelling ratio was calculated as ($m_s$ – $m_{d2}$) / $m_{d2}$. The sol fraction, representing the non-crosslinked mass fraction in the polymer network, was calculated as ($m_{d1}$ – $m_{d2}$) / $m_{d1}$.

### 2.6. Scanning electron microscopy

Hydrogel microstructure was assessed using Scanning Electron Microscopy (SEM, Phenom, Fisher Scientific). Disc-shaped hydrogels were prepared as discussed in Section 2.3. After swelling in PBS, hydrogels were flash-frozen in liquid nitrogen. The internal hydrogel structure was exposed by cryofracture, followed by lyophilization. Hydrogels were then fixed on SEM stubs using carbon tape. Following 6 nm gold-sputter coating, imaging was performed.

### 2.7. Mechanical analysis

Compression modulus of GTA hydrogels was determined using Dynamic Mechanical Analysis (DMA, Q800, TA Instruments, Etten-Leur, NL). A ramp-force protocol was set, increasing force up to 18 N at a rate of 3 N/min. All DMA measurements were performed at room temperature. A stress-strain curve was generated for sam-

ples and the coefficient in the linear viscoelastic (LVE) range was retrieved, representing the compression modulus.

### 2.8. Rheological analysis

Rheological measurements were carried out using a rheometer (Discovery HR-2, TA instruments, Etten-Leur, NL) with a 20 mm parallel plate geometry at RT. Amplitude sweeps were performed at a frequency of 1 Hz and shear strain from 0.1% to 100%. Frequency sweeps were performed at a strain of 1% and frequency range from 0.1 Hz to 100 Hz. Cyclic strain-recovery was performed by exposing gels to alternating intervals of low strain (2 minutes, 1% strain) and high strain (1 minute, 100% strain). G' and G" were recorded to assess viscoelastic behavior of hydrogels. Mesh size calculations based on the rubber elasticity theory were performed using the experimentally determined rheology data according to the following formula [39,40]:

$$mesh\ size\ \xi\ = \left(\frac{G' \times N_A}{R \times T}\right)^{-\frac{1}{3}}$$

Where G' is the storage modulus (Pa), $N_A$ is the Avogadro constant, R is the molar gas constant and T is the temperature.

### 2.9. Drug loading and in vitro release

Following washing of crosslinked gels, samples were dried and incubated in a bupivacaine HCl solution at 37 °C. In a next step, hydrogels were treated with 0.1 M $NaHCO_3$ (pH 8.5) containing glycerol to induce *in situ* alkaline crystallization of bupivacaine. Ring-shaped hydrogel loaded with bupivacaine HCl and crystallized bupivacaine were tested for release in 0.01 M citrate buffer (pH 6) at 37°C. At time points of interest up to 168 hours, aliquots were collected and replaced with the same volume of fresh buffer. After 168 hours the hydrogels were incubated in 0.15% collagenase II solution in 0.01 M citrate buffer (pH 6) until they had completely degraded to determine total drug content [41].

Bupivacaine content of samples was analyzed using HPLC (Prominence LC20A, Shimadzu Corp, Kyoto, Japan) with Waters Acquity HSS T3 1.8 $\mu$m column, 100 mm (Waters Chromatography, Etten-Leur, NL). Mobile phase A and B consisted of 10 mM ammonium formate (pH 2.4) and acetonitrile, formic acid and water in 96:0.2:5 ratio (UV-vis detection at 262 nm), respectively, utilizing a previously described method [42]. . A standard ranging from 5 $\mu$g - 5 mg/mL bupivacaine HCl in 0.01 M citrate buffer (pH 6) was used to convert sample absorbance to concentration.

### 2.10. In vitro cytocompatibility

Cytocompatibility of hydrogels (50 $\mu$L volume) and drug-loaded hydrogels (50 $\mu$L volume) was tested using a direct-contact method. NIH3T3 mouse fibroblasts and human mesenchymal stem cells (hMSCs) were seeded at a density of 8000 cells/ well in a 24-wells plate. Cells were cultured up to 80% confluence in a humidified incubator set at 37 °C with 5% $CO_2$ using Alpha-Minimum Essential Medium (Alpha-MEM, Gibco, Fisher Scientific) supplemented with 10% fetal bovine serum (FBS), 1% ascorbic acid and 1% penicillin-streptomycin. Medium was replaced every three days. Hydrogels discs were placed on top of the cells. The control group consisted of cells exposed only to culture medium. After 24 and 48 hours of exposure, cell metabolism was quantified using an Alamar Blue assay. Fluorescence was measured using a Fluoroskan Ascent plate reader (ThermoFisher Scientific) with excitation and emission set at 544 and 570 nm, respectively. Cell viability was assessed using a Live/Dead assay (Invitrogen), staining live cells green with Calcein acetoxymethyl ester (AM) and dead cells red with ethidium homodimer. A stock solution of 2 $\mu$M Calcein AM and 4 $\mu$M Ethidium homodimer in PBS was prepared. Upon reaching the desired duration of cell exposure to gels, gels and culture medium were removed and cells were washed with PBS. Live/Dead staining stock solution was added to the wells and incubated at 37 °C for 30 minutes prior to imaging. Live cell counts were normalized to controls. Imaging was performed using an inverted fluorescence microscope (Olympus BX51, Olympus, Germany). Hydrogels were tested in quintuplicate unless stated otherwise. Three images were taken for each sample to accurately represent cell compatibility. Images were analyzed using ImageJ (NIH, Bethesda, Maryland, USA). All groups were compared to control.

### 2.11. In vitro degradation assay

To assess hydrolytic degradation, the dry mass of disk-shaped hydrogel samples was recorded, after which hydrogels were submerged in 1 mL of PBS containing 0,01% sodium azide to prevent microbiological growth. In the enzymatic degradation assay, hydrogels were submerged in collagenase II at 2 EU/mL (Worthington Biochemical Corp) in PBS with 0,01% sodium azide at 37 °C to simulate surgical wound enzyme concentrations [43–45]. The collagenase solution was replaced every three days to maintain constant enzymatic activity. In both the enzymatic and hydrolytic degradation assay, gels were collected at predetermined times and the remaining dry mass was recorded. Mass loss was expressed as (remaining mass/ original mass) * 100.

### 2.12. Ex vivo implantation

Fresh cadaveric female sheep specimens (age 5-7 years) were obtained for *ex vivo* implantation of twenty ring-shaped hydrogels by a board-certified spine surgeon (JJV). Sheep surgery was performed in the prone position. A midline incision was performed over the spinous processes, paraspinal muscles were dissected and moved laterally to allow for a clear view of lamina, spinous- and transverse processes. A hole was drilled into the pedicle of the lumbar vertebrae. Next, the ring-shaped hydrogel was mounted on a polyaxial pedicle screw and the screw was tightened according to clinical practice. Mechanical performance of the ring was assessed macroscopically. Specific attention was paid to cracks in- or rupturing of the hydrogel. If no damage was observed, the screw was overtightened and ring performance was scored again. Rings were then explanted and again assessed for signs of failure.

### 2.13. Statistical analysis

All statistical analysis was performed using Prism 8.0 (GraphPad Software Inc, San Diego, CA, USA). All data are presented as mean ± standard deviation. Data was analyzed using a one-way (or two-way when necessary) analysis of variance (ANOVA) combined with Tukey's honestly significant difference to correct for multiple comparisons. A significance level of $p < 0.05$ was used.

## 3. Results and discussion

### 3.1. Synthesis of gelatin-tyramine and oxidized beta-cyclodextrin

Tyramine functionalized gelatin (GTA) was obtained by carbodiimide-mediated coupling of tyramine to the carboxylic groups present on the gelatin backbone (Fig. 1B). The coupling reaction involves the formation of an amine-reactive *N*-hydroxysuccinimide (NHS) ester which is susceptible to hydrolysis [46]. Performing the reaction at low temperature (*e.g.* 4 °C) minimizes hydrolysis, increasing the half-life of the active NHS ester and thereby the efficiency of the coupling reaction [46,47]. Because gelatin is soluble at temperatures above 37 °C,

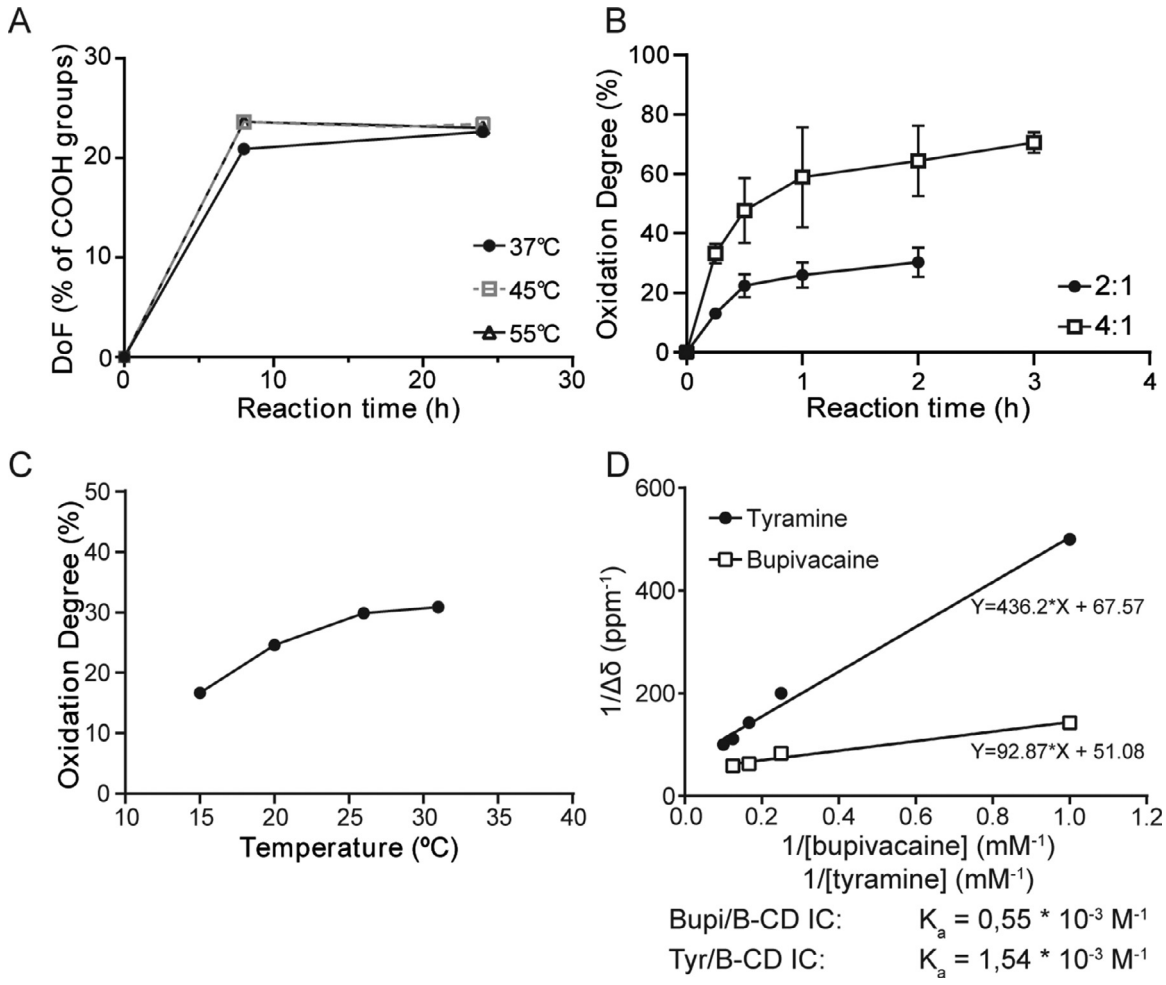


**Fig. 2.** Effect of reaction time and temperature on the synthesis of the hydrogel's precursors. **A** Effect of reaction time and temperature on the EDC-mediated coupling of tyramine to gelatin carboxylic groups, using a [tyramine HCl]:[COOH] ratio of 4:1, [EDC]:[NHS] ratio of 2:1 and gelatin at 1.67%. A single reaction per temperature was performed. **B** Effect of [$NaIO_4$]:[B-CD] ratio and reaction time on the degree of oxidation degree of B-CD at 25 °C. Three reactions per ratio were performed. **C** Effect of temperature on the degree of oxidation of B-CD, using a [$NaIO_4$]:[B-CD] ratio of 2:1 and reaction time of 1 hour. A single reaction per temperature was performed. **D** Benesi Hildebrand plot quantifying the association constant ($K_a$) interaction between B-CD and tyramine or bupivacaine in DMSO determined from $^1$H NMR spectra. B-CD concentrations were kept constant at 11 mM and combined with increasing bupivacaine concentrations (1-8 mM) or tyramine concentrations (1-10 mM).

the coupling reaction cannot be conducted at low temperature. To assess the effect of reaction temperature and time on the degree of functionalization (DoF), the coupling reaction was conducted at three different temperatures, namely 37 °C, 45 °C and 55 °C. For each temperature, the degree of functionalization was determined at 8 hours and 24 hours of reaction. The amount of tyramine conjugated to gelatin was quantified by measuring the absorbance at 275 nm, as previously described [24]. The DoF of the hydrogels resulting from reactions performed in the temperature range 37-55 °C did not significantly differ between temperatures and between 8 and 24 hours of reaction (Fig. 2A). Carboxylic groups are present in gelatin type A at a concentration of 780-800 $\mu$mol per gram [36]. A 4:1 excess of tyramine was added during the reaction. Based on these results, the coupling reaction temperature was then set to 45 °C and the time to 8 hours, resulting in a degree of functionalization of 22.3% (±1.4%) of the carboxylic groups of gelatin, which equals to 176 $\mu$mol tyramine / g GTA.

Oxidized B-CD (oB-CD) was prepared using sodium periodate ($NaIO_4$), which induces the cleavage of vicinal glycols leading to the formation of dialdehyde functionalities. (Fig. 1B-ii). The extent of oxidation was monitored for up to 3 hours using a [$NaIO_4$]:[B-CD] ratio of 2:1 and 4:1, and quantified using $^1$H NMR (Fig. 2B and Fig. S1). The aldehyde content displayed a fast increase when using a [$NaIO_4$]:[B-CD] ratio of 4:1, especially after 1 hour of reaction. A similar curve shape was observed when using a ratio of 2:1, though the aldehyde content was lower in comparison to the one obtained with the ratio 4:1. Because the 2:1 ratio yielded a slower increase in degree of oxidation and a lower final aldehyde content and thus better control over the reaction, this ratio was selected for further investigations.

To evaluate the effect of temperature on the oxidation degree, the reaction was monitored for 1 hour in a temperature range from 15 °C to 35 °C (Fig. 2C). When the reaction was conducted at room temperature and at a [$NaIO_4$]:[B-CD] ratio of 2:1, the oxidation degree was 23.7% (±1.5%), as measured by NMR (Fig. S1). This oxidation degree was chosen to provide sufficient water solubility of oB-CD, while simultaneously allowing a large number of oB-CD molecules to be attached to gelatin chains through Schiff base formation between the amino groups on gelatin and aldehyde functionalities on oB-CD. This way, the main function of oB-CD was to provide additional elasticity to the network *via* guest-host complexation with tyramine moieties grafted on gelatin (Fig. 1B).

### 3.2. Preparation and characterization of GTA / oB-CD hydrogels

As shown in Figure 1, dual-crosslinked hydrogels were prepared by mixing GTA with oB-CD and crosslinked via exposure to visible

light, using riboflavin (RB) and sodium persulfate (SPS) as photoinitiating system. Under the influence of visible light, riboflavin and sodium persulfate induce the formation of di-tyramine crosslinks between tyramine moieties grafted onto the gelatin backbone [28]. The exposure of riboflavin to visible light induces photo-excitation of riboflavin, which promotes the formation of tyrosyl radicals from the grafted tyramine moieties and tyrosine residues present on the gelatin backbone. Di-tyramine bonds are then obtained by the coupling of two adjacent tyrosyl radicals [48]. In addition, imine bonds formed through Schiff base reaction between the aldehyde groups on oB-CD with primary amines groups on gelatin, and inclusion complexes formed between the oB-CD cavity and tyramine moieties grafted on the gelatin backbone directly after mixing of stock solutions. Concentration-dependent additional cross-linking by oB-CD was confirmed with dynamic mechanical analysis.

The formation of inclusion complexes of B-CD with a variety of guest molecules (including tyramine) has been previously investigated by $^{1}$H NMR spectroscopy [49]. Different values of association constants have been reported in the literature for inclusion complexes between B-CD and bupivacaine. The stability of the formed complex depends highly on the pH and the temperature used, and values obtained by different techniques are difficult to compare (*e.g.* HPLC vs NMR) [49,50]. Further, the stability of the complex depends on the type of substituents on the cyclodextrin core. For example, sulphobuthylether-B-CD forms a more stable complex with bupivacaine compared to B-CD and bupivacaine [51]. The experiment in our study was performed on B-CD and not oB-CD, as it was hypothesized that aldehyde groups on oB-CD would already have reacted with amine groups present on gelatin at the time of bupivacaine loading.

To assess the stability of complex formed between bupivacaine with B-CD and of tyramine with B-CD, their inclusion into the B-CD cavity was investigated by NMR spectroscopy (Fig. S2 and S3). The association constant ($K_a$) was $0.55 \times 10^{-3}$ $M^{-1}$ for bupivacaine/ B-CD and $1.54 \times 10^{-3}$ $M^{-1}$ for tyramine/ B-CD, as determined using a Benesi-Hildebrand plot (Fig. 2D)[29]. As the Ka of tyramine exceeds the bupivacaine Ka almost three-fold, little competition between tyramine and bupivacaine for the B-CD cavity is expected.

Swelling ratio and sol fraction were determined to understand the effect of the hydrogel composition on its physical properties. The swelling ratio is a measure of the amount of water a hydrogel can uptake, expressed as a ratio to the hydrogel's dry weight and is predominantly determined by the crosslinking density of the polymer network. Other factors influencing swelling ratio are temperature, pH, ionic strength of swelling medium and the presence of hydrophilic or hydrophobic groups [52]. With diffusion-based drug loading, the swelling ratio directly influences the amount of drug the hydrogel can encapsulate. We therefore aimed for a crosslinking density that leads to a robust hydrogel but allows for sufficient uptake of solubilized drug. Firstly, the effect of GTA concentration on hydrogel properties was investigated (Fig. 3A-i). To evaluate the effect of GTA concentration, hydrogels were prepared by fixing the concentration of RB and SPS to 2 mM and 20 mM, respectively, and the irradiation time to 30 min. The swelling ratio was significantly lower for hydrogels with a GTA content of 20 wt.% compared to samples with GTA 15 wt.%. No significant difference was observed for hydrogels with a GTA content between 5 and 15 wt.%. Next, we determined the sol fraction of hydrogels with a GTA content from 5 to 20 wt.%, as a measure of the non-crosslinked portion of the polymer mass [53]. Increasing GTA concentration from 5 to 20 wt.% led to significantly lower sol fractions and slightly lower swelling ratio (Fig. 3A-i and 3A-ii). Based on these results, for further experiments GTA concentration was set at 20 wt.% as it displayed low swelling ratio and sol fraction, indicating a more efficient crosslinking compared to the other formulations. To study the effect of oB-CD concentration on the swelling ratio, hydrogels with increasing concentrations of oB-CD up to 6 wt.% were investigated. Increasing the oB-CD concentration led to a decrease in swelling ratio, likely due to the formation of additional crosslinks between oB-CD and GTA (Fig. 3B-i). A significant decrease in swelling ratio was observed for hydrogels with an oB-CD content up to 4 wt.%. Samples containing 4 wt.% and 6 wt.% oB-CD did not exhibit any significant difference in swelling ratio, while the sol fraction significantly increased for oB-CD content from 0-6 wt.%, suggesting a potential saturation of the hydrogel network with oB-CD and subsequent washout of excess oB-CD, resulting in increased sol fraction. (Fig. 3B-ii). Based on the data from swelling ratio and sol fraction, the oB-CD concentration was therefore fixed at 4 wt.%. In a similar fashion, the influence of SPS concentration on gel formation was evaluated. In the absence of SPS, no gels were formed. Increasing the SPS concentration from 10 mM to 40 mM led to significant decreases in swelling ratio (Fig. 3C), as previously described for silk fibroin hydrogels photo-crosslinked using RB/SPS in presence of visible light [28]. Swelling ratio of hydrogels containing 20 mM and 40 mM SPS did not display any significant difference (Fig. 3C). To minimize SPS content yet allowing efficient crosslinking, SPS concentration was therefore fixed at 20 mM. Self-standing hydrogels could be formed following exposure to visible light for 5 minutes. While hydrogels were formed within 5 minutes of irradiation, increasing the irradiation time led to significant decreases in swelling ratio, suggesting that a longer reaction time is required to achieve a complete crosslinking. After 30 minutes of irradiation, no more changes in the swelling ratio were observed (Fig. 3D) and therefore the irradiation time was fixed at 30 minutes for future experiments. These data show that the current photo-crosslinking system allows temporal control of crosslinking, in contrast to systems using enzyme-mediated crosslinking that starts upon mixing hydrogel ingredients together [24]. RB concentration was fixed at 2 mM based on previous investigations [28]. To confirm that this concentration gives the best results with SPS at 20mM and an irradiation time of 30 minutes, hydrogels were prepared by varying RB from 1-4 mM. No significant changes in either swelling ratio or sol fraction were observed when using RB concentrations of 1 mM, 2 mM and 4 mM (Fig. S4). These results show that GTA, oB-CD and SPS concentration as well as irradiation time are important determinants in the network formation. Riboflavin concentration did not affect the crosslinking efficiency in the ranges investigated.

### 3.3. Shear and compressive mechanical properties of GTA / oB-CD hydrogels

Implantation of the hydrogel with a pedicle screw onto a vertebra exerts considerable compressive and shear strain on the hydrogel especially at final tightening of the screw (Fig. 1B). To assess the ability of the GTA / oB-CD hydrogel to withstand shear and compression forces during implantation, we assessed its mechanical properties. The compressive modulus determined by dynamic mechanical analysis was affected by the oB-CD content and irradiation time (Fig. 4A-i) The compressive modulus increased from 375 kPa (± 57) to 621 kPa (± 226) with increasing oB-CD content (*i.e.,* between 0 wt.% and 6 wt.%, $p < 0.05$). Furthermore, as irradiation time is an important determinant in network formation, its effect on compression modulus was tested by varying the exposure time to visible light from 5 to 30 minutes (Fig. 4A-ii) while maintaining the oB-CD content at 4 wt.%. Samples prepared by using an irradiation time of 5 min displayed the lowest compressive modulus (168 kPa ± 30), which is in agreement with the swelling ratio, as shown in Fig. 3D. Samples photo-crosslinked for 10, 20 and 30 minutes exhibited a linear increase of compressive modulus from 328 kPa (± 29) to 552 kPa (± 138). The compressive moduli of these hy-

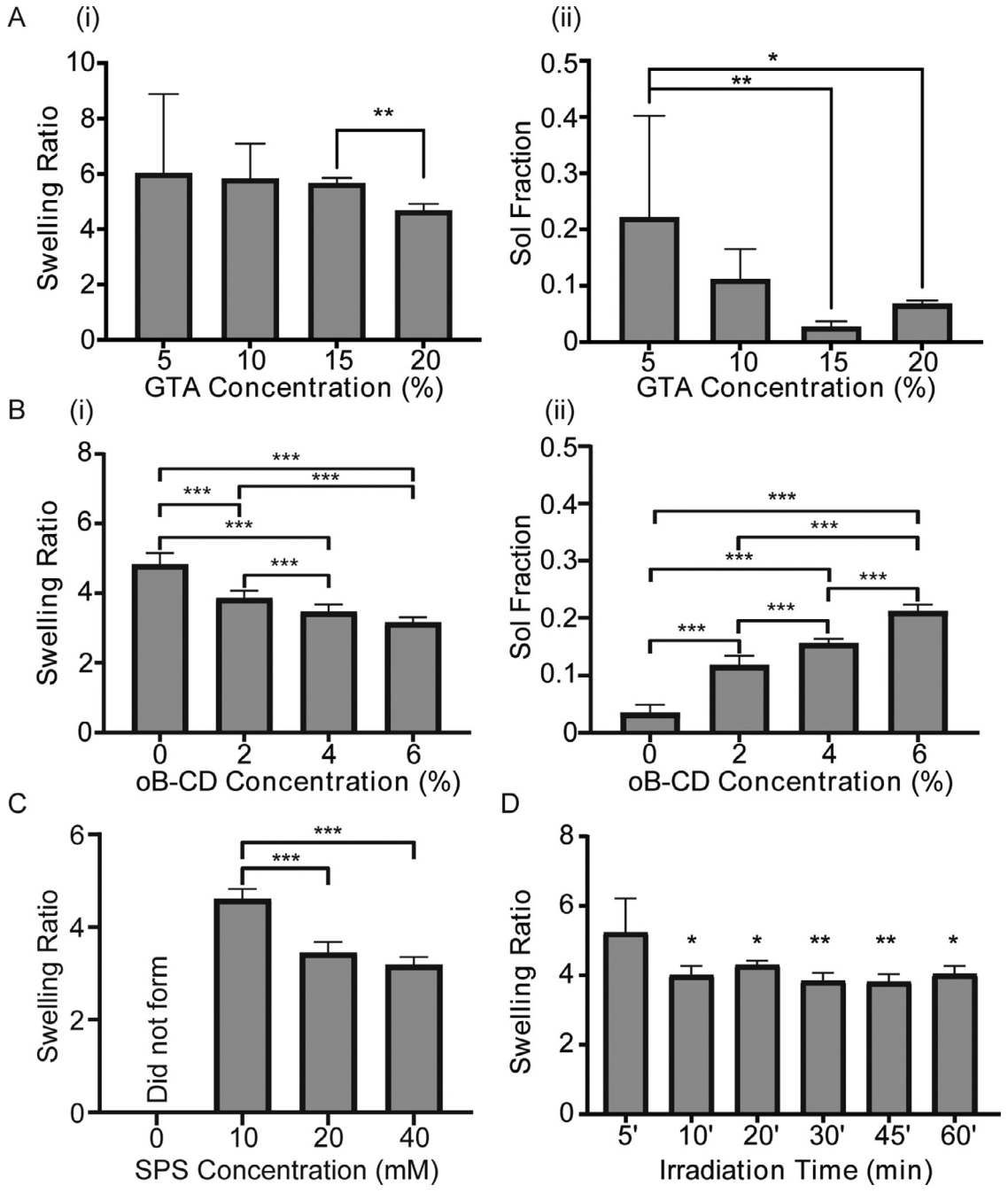


**Fig. 3.** Characterization of swelling behavior and sol fraction of GTA/oB-CD hydrogels. **A** Effect of GTA concentration (wt.%) on swelling ratio (i) and sol fraction (ii) of 100 $\mu$L disc-shaped hydrogels ($N = 6$). Hydrogels did not contain oB-CD, irradiation time was set to 30 minutes, SPS concentration at 20 mM and RB at 2 mM. **B** Effect of oB-CD concentration (wt.%) on swelling ratio (i) and sol fraction (ii) of 100 $\mu$L disc-shaped hydrogels at fixed GTA concentrations of 20 wt.%, RB 2 mM and SPS 20 mM, irradiation time 30 min. **C** Effect of SPS concentration on swelling ratio of disc-shaped hydrogels containing 20% GTA, 4% oB-CD and 2 mM RB. Gels were irradiated for 30 minutes. **D** Effect of irradiation time on hydrogel swelling ratio in disc-shaped hydrogels containing 20% GTA, 4% oB-CD, 20 mM SPS and 2 mM RB. N = 4-6 for all compositions. Data was analyzed using one-way ANOVA, paired with Tukey's test. * $p < 0.05$, ** $p < 0.01$, *** $p < 0.001$.

drogels are considerably higher than other gelatin-based hydrogels, such as gelatin-methacryloyl (GelMA) hydrogels. Indeed, the compressive modulus of GelMA hydrogels varied between 2 kPa for a gelatin content of 5 wt.% up to 180 kPa for hydrogels containing 30 wt.% GelMA, depending on crosslinking agent and degree of substitution [54,55]. This difference is likely due to the mechanism of hydrogel formation, which in the case of GelMA hydrogels occurs via chain growth polymerization of the methacryloyl groups [54]. GTA hydrogels are crosslinked by the formation of dityramine bonds, which lead to a tighter network in comparison to GelMA hydrogels [28,30]. In addition, the present GTA hydrogel contains B-CD which is connected to the gelatin chains via Schiff base formation and guest-host interactions.

Next, rheological measurements were conducted to investigate the viscoelasticity of the GTA/oB-CD hydrogels. Strain sweep of GTA/ oB-CD hydrogels displayed a quite broad linear viscoelastic region (LVE) with network breakdown at high strains (Fig. 4B). Further, the shear modulus increased with increasing content of oB-CD in the network; however, oB-CD content did not impact the amplitude at which the network collapsed (Fig. S5). To assess the

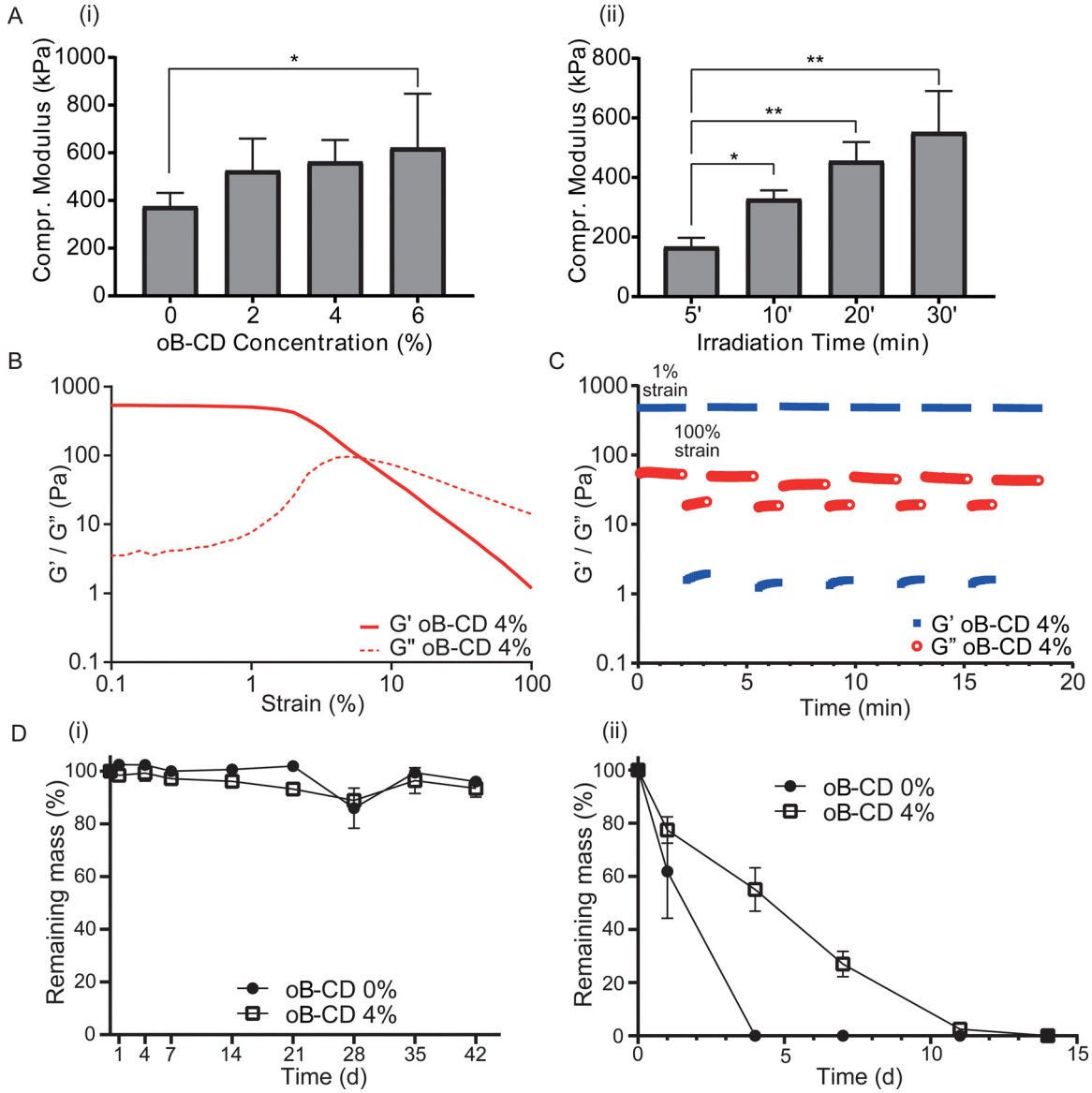


**Fig. 4.** Mechanical characterization of GTA/oB-CD hydrogels, and investigation of hydrolytic and enzymatic degradation. **A** Effects of (i) oB-CD concentration (30 minutes of irradiation) and (ii) irradiation time (gels containing 4% oB-CD) on compression modulus of disc-shaped hydrogels containing 20% GTA, 20 mM SPS and 2 mM RB. **B** Strain sweep of hydrogels containing 20% GTA and 4% oB-CD hydrogels. A representative sample taken from $N = 3$ is shown. **C** Rheological properties of hydrogels containing 20% GTA, 4% oB-CD hydrogels during cyclic strain-recovery. Average result of $N = 5$ is shown, standard deviations have been removed for clarity. **D** Effect of oB-CD content on (i) hydrolytic and (ii) enzymatic degradation. 50 $\mu$L disc-shaped hydrogels were incubated in PBS or collagenase II 2 EU/mL solution for hydrolytic and enzymatic degradation, respectively. Gels contained 20% GTA, 20 mM SPS, 2 mM RB, 0-4% oB-CD and were irradiated for 30 minutes. * $p < 0.05$, ** $p < 0.01$.

recovery of material properties following network breakdown at high strain (100 %), GTA/ oB-CD hydrogels were subjected to shear strain cycles of high (100%) and low (1%) strain (Fig. 4C). At low strain, GTA/ oB-CD hydrogels containing 4% oB-CD exhibited a typical gel behavior with the elastic modulus higher than the viscous modulus (G' > G"). In the next cycle, when hydrogels were subjected to a high shear (100%), the elastic modulus decreased from 480 Pa to 1.8 Pa, indicating a transition from a solid-like to a viscous-like behavior. After decreasing the strain to its initial value, a rapid and complete recovery of G' to the initial levels was observed and it did not change over several cycles. This behavior can be attributed to the combination of the permanent photo-crosslinking with the reversible imine bonds and guest-host interactions, which together contribute to the formation of a strong and self-recovering matrix. We deem these properties desirable for the successful implantation of the hydrogel during musculoskeletal surgery.

### 3.4. Enzymatic and hydrolytic degradation

The use of naturally-derived polymers as drug delivery carriers allow shorter *in vivo* degradation time following drug release, a distinct advantage compared to longer degradation times observed when using synthetic polymers such as poly(lactic-co-glycolic) acid and poly(caprolactone) to prepare drug delivery formulations [56,57]. Gelatin can undergo hydrolytic degradation, proceeding *via* the cleavage of amide bonds. Furthermore, its Pro – X – Gly – Pro (where X is a neutral amino acid) sequences make gelatin susceptible to enzymatic degradation. These sequences can be cleaved by matrix metalloproteinases, such as collagenase II, naturally present in the body [58]. To simulate physiological conditions, hydrolytic degradation was investigated by incubation of GTA/oB-CD hydrogels in PBS buffer (pH 7.4) at 37 °C. The hydrolytic degradation was monitored by measuring hydrogels' remaining mass at fixed time points over a period of 42 days. As ex-

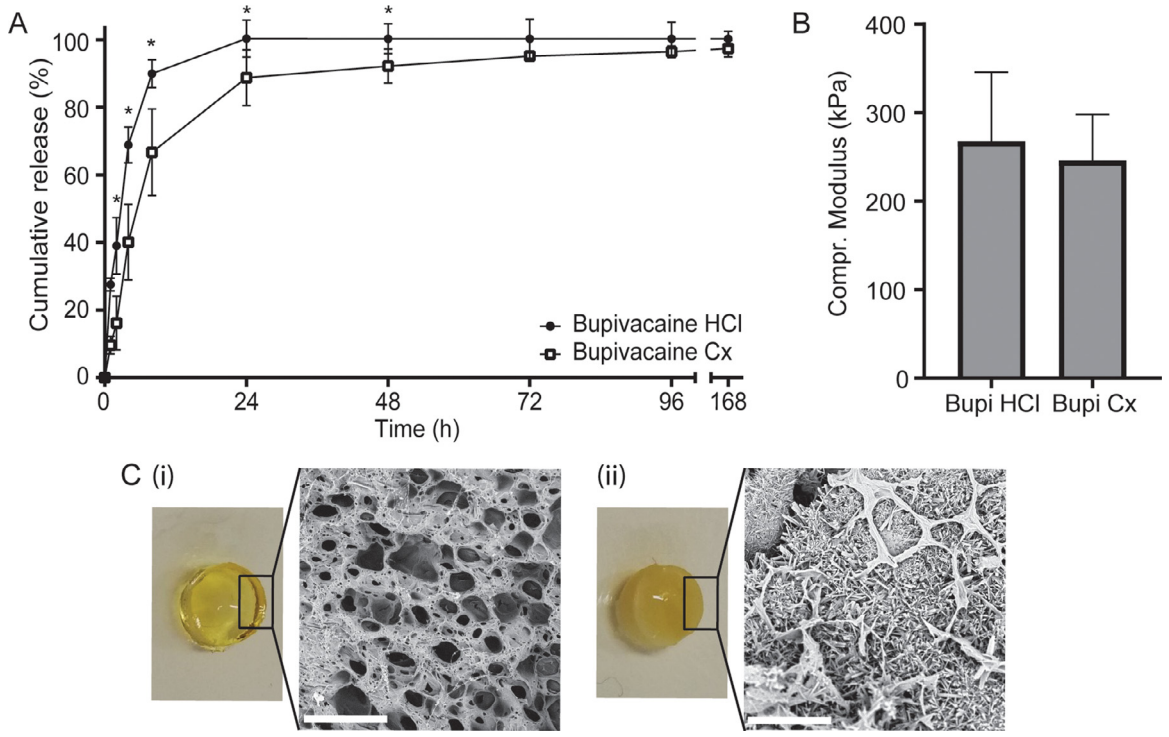


**Fig. 5.** Bupivacaine release from GTA/oB-CD hydrogels. **A** Release of bupivacaine HCl and bupivacaine crystals from ring-shaped hydrogels. Release is plotted as the percentage of total bupivacaine content in the hydrogels. Total bupivacaine content was determined by hydrogel degradation after 168 hours of release. Data are presented as mean ($N = 5$) with standard deviation as error bars. Data was analyzed using an independent samples t-test at each time point. **B** Effect of bupivacaine crystals on compression modulus. Data was analyzed using an independent-samples T-test ($p > 0.05$). **C** Scanning electron microscope (SEM) images of hydrogels with and without bupivacaine crystals (scale bar 100 $\mu$m).

pected, no decrease in hydrogel weight was observed at the physiological conditions used. This resistance of gelatin hydrogels to hydrolytic degradation is in agreement with previously described hydrogels and likely due to the stability of peptide bonds at physiological conditions [59]. The rate of hydrolytic degradation did not differ between hydrogels with and without 4% oB-CD (Fig. 4C-i). As gelatin is susceptible to enzymatic degradation, this was studied at 37 °C in a simulated body fluid containing physiological levels of collagenase II (PBS, collagenase II 2 EU/mL) [43]. Hydrogels that did not contain oB-CD were completely degraded in four days, whereas in presence of oB-CD the degradation time increased to eleven days (Fig. 4C-ii). This extended duration of degradation may be due to the presence of bulky oB-CD moieties that might hinder the diffusion of the enzyme within the hydrogel and the accessibility of the enzyme-cleavable sequences in the gelatin chains [60]. With a molecular weight for collagenase of approx. 130 kDa, the molecule's radius is estimated to be at least 3 nm [41,61]. As a result, the enzyme will first cleave the outer gelatin chains, slowly reaching the inner part of the hydrogels leading to a complete degradation. Indeed, calculations based on the rubber elasticity theory showed that the presence of oB-CD leads to a decrease in mesh size, with mesh size of 11.1 ± 0.8 nm and 8.1 ± 1.2 nm for hydrogels without oB-CD and with 6% oB-CD, respectively.

### 3.5. Sustained release of bupivacaine from GTA / oB-CD hydrogels

Following implantation during surgery, the hydrogel was designed to deliver the local anesthetic bupivacaine in a sustained manner. Drug loading was performed by immersing ring-shaped hydrogels in a bupivacaine HCl solution (50 mg/mL) for 24 hours at 37 °C. The release profile of bupivacaine from the GTA/oB-CD gels was monitored for 168 hours and displayed a considerable initial burst followed by a fast release beyond 24 hours (Fig. 5A). Decreasing an initial burst of LA from sustained release formulations is a major developmental challenge [10]. Indeed, burst release might lead to sudden high local or serum levels of bupivacaine, putting patients at risk of adverse effects [20]. Conversely, initial burst release inherently decreases the amount of drug available in the hydrogel to provide analgesia after the burst release has been washed out. To decrease this initial burst and achieve a sustained release of bupivacaine, drug crystals were formed inside the hydrogel matrix by pH-induced drug crystallization. This way, crystal dissolution would act as an additional rate-limiting step in the diffusion of the drug from the hydrogel. Previous studies showed that pH-induced drug crystallization enable high drug loading and prolonged release [62]. To induce *in-situ* drug crystals formation, hydrogels were first incubated in a solution of bupivacaine HCl, followed by incubation in a sodium bicarbonate/ glycerol mixture for 2 hours at 37°C. Prior to crystal formation, bupivacaine HCl content per ring was 55.5 ± 2.9 mg. Following alkaline-promoted crystallization, hydrogels contained a bupivacaine dose of 49.8 ± 3.5 mg. The release profile of hydrogels containing crystallized bupivacaine was characterized by a moderate decrease in initial burst release as compared to bupivacaine HCl ($p < 0.05$). The bupivacaine alkaline crystallization procedure led to a formulation with a burst release of 66.7 ± 12.9% of total dose after 8 hours, compared to 90.0 ± 4.1% of total dose released from hydrogels containing bupivacaine HCl. Release from hydrogels containing crystallized bupivacaine was significantly slower compared to hydrogel containing bupivacaine HCl up to 48 hours after initial drug release. After 168 hours of release, hydrogels were collected and the residual bupivacaine content was determined. Hydrogels subjected to *in situ* crystallization had 2.6 ± 2.5% of total drug content left in the matrix (Fig. 5A). No bupivacaine was left in hydrogels containing bupivacaine HCl beyond 24 hours, demonstrating the beneficial effect of bupivacaine crystals in slowing down release. Although hydro-

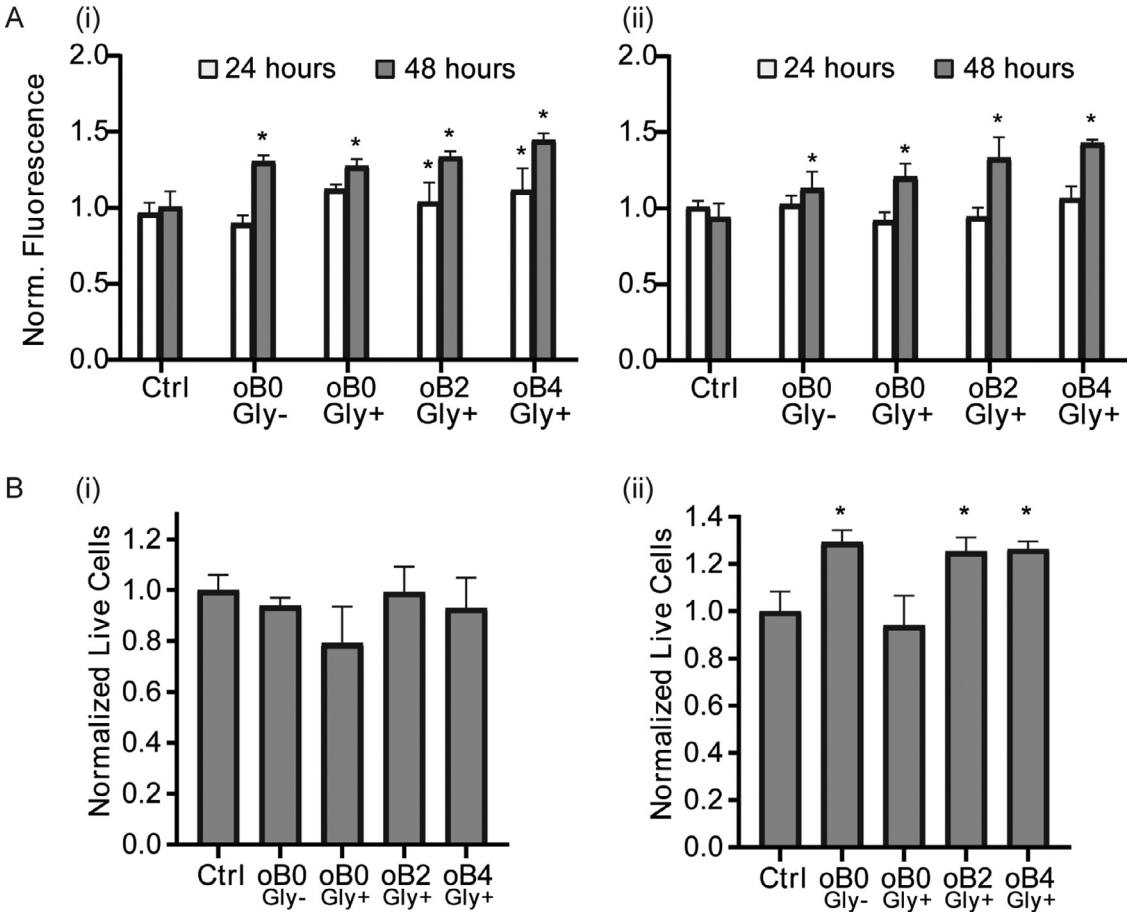


**Fig. 6.** Metabolic activity and viability of MSCs and fibroblasts. A Metabolic activity of NIH3T3 fibroblasts (i) and MSCs (ii) determined by Alamar Blue assay after 24 and 48 hours of exposure to GTA hydrogels, with (Gly+) or without (Gly-) glycerol, and containing increasing concentrations of oB-CD (0-4 wt.%). All values have been normalized to controls. B Live/Dead assay of NIH3T3 fibroblasts (i) and MSCs (ii) after 48 hours of exposure to hydrogels with (Gly+) or without (Gly-) glycerol, and containing increasing concentrations of oB-CD (0-4%). Viability is expressed as live cell count normalized to control wells. Controls consisted of monolayer cells exposed to culture medium only in all cases. Data are presented as mean ($n = 4$) with standard deviation. Data was analyzed using one-way ANOVA. All groups were compared to controls. * $p < 0.05$.

gels containing crystallized bupivacaine had only 11% of total dose left after 24 hours, we believe this concentration might be anesthetically effective as the analgesic effect will likely depend on local concentration and clearance of bupivacaine. As pedicle screws and thus hydrogels will be closely surrounded by muscle tissue following surgery, literature on bupivacaine clearance from muscle might be indicative of in vivo performance. Indeed, in a previous study performed by McDonald et al. muscle tissue concentrations were quantified using microdialysis in rats following administration of bupivacaine HCl infiltration or a bupivacaine microparticle formulation. Despite the *in vitro* release of the microparticles being limited to 30 hours, tissue concentrations equaling those obtained shortly after bupivacaine HCl infiltration were obtained until four days after administration [63]. Moreover, bupivacaine elimination half-life from swine skeletal muscle was reported to be 82 minutes [64].Further, in clinical practice, instrumented spinal surgery always involves implantation of four or more pedicle screws which enables the implantation of at least four hydrogels. Taken together, implantation of multiple hydrogel rings, as well as limited local clearance rates that possibly lead to accumulation of bupivacaine at the surgical site, could both increase the likelihood of analgesic effect beyond 24 hours.

Further, to assess the effect of bupivacaine crystals on stiffness, the mechanical properties of hydrogels containing bupivacaine crystals and bupivacaine HCl were investigated by dynamic mechanical analysis. The presence of bupivacaine crystals did not significantly affect the compression modulus of the hydrogel (Fig. 5B). Because bupivacaine is crystallized after the network formation, there is no interference with the crosslinking. As a consequence, bupivacaine crystals can only grow within the space available in the hydrogel matrix. The presence of bupivacaine crystals inside the porous structure of the hydrogel was confirmed using SEM (Fig. 5C).

### *3.6. Cytocompatibility of GTA Hydrogels for sustained bupivacaine release*

To determine the cytocompatibility of the developed hydrogel formulation, the metabolic activity and viability were determined by culturing human mesenchymal stromal cells (MSCs) and NIH3T3 fibroblasts in presence of GTA hydrogels for 48 hours. MSCs and fibroblasts were selected, as fibroblasts and differentiated MSCs make up the majority of cells present in the orthopedic wound [65]. Indeed, following implantation, the hydrogel for LA delivery comes into contact with various tissues such as bone, muscle, tendon, ligament and fascia. As shown in Fig. 6A, cell metabolic activity was quantified using an Alamar Blue assay on cells cultured in contact with hydrogels contained increasing concentrations of oB-CD. Metabolic activity was quantified after 24 and 48 hours of culture. Significant differences were observed in MSCs and fibroblast metabolic activity compared to controls (Fig. 6A). In all groups exposed to hydrogels, cell metabolism increased compared to controls after 48 hours of culture. This effect could be due to the presence of RB, as RB has been linked

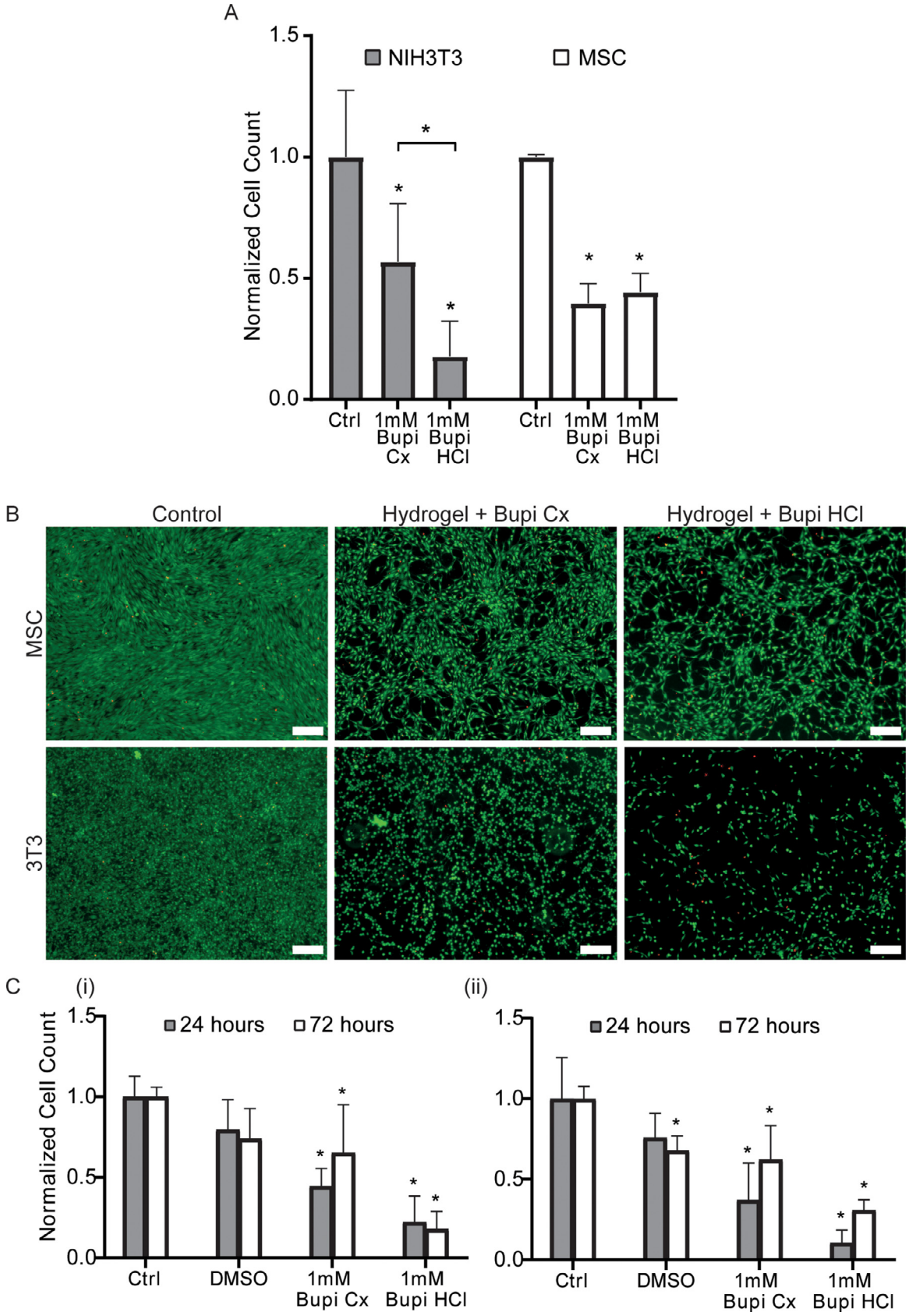


**Fig. 7.** Cytocompatibility of GTA/oB-CD hydrogels containing bupivacaine. A Live/Dead assay of MSCs and NIH3T3 fibroblasts following 24 hours of exposure to gels loaded with bupivacaine crystals (Cx) or bupivacaine HCl. All values have been normalized to control live cell count. B Representative fluorescent microscope images of live/dead staining of MSCs and NIH3T3 fibroblasts, after 24 hours of exposure to gels loaded with bupivacaine crystals (Cx) or bupivacaine HCl (scale bar 200 $\mu$m). C Live/Dead assay of MSCs (i) and NIH3T3 fibroblasts (ii) after 24 hours of exposure to culture medium containing 1 mM bupivacaine HCl in DMSO, 1 mM bupivacaine crystals (Cx) in DMSO, and equivalent volumes of DMSO in culture medium. 72 hours cells were exposed to solutions for 24 hours, followed by 48 hours of recovery. All values have been normalized to control live cell count. Controls consisted of monolayer cells exposed to culture medium only in all cases. Data are presented as mean ($n = 5$) with standard deviation as error bars. Statistical analysis was performed using a one-way ANOVA. All groups were compared to controls. $^{*}$ $p < 0.05$.

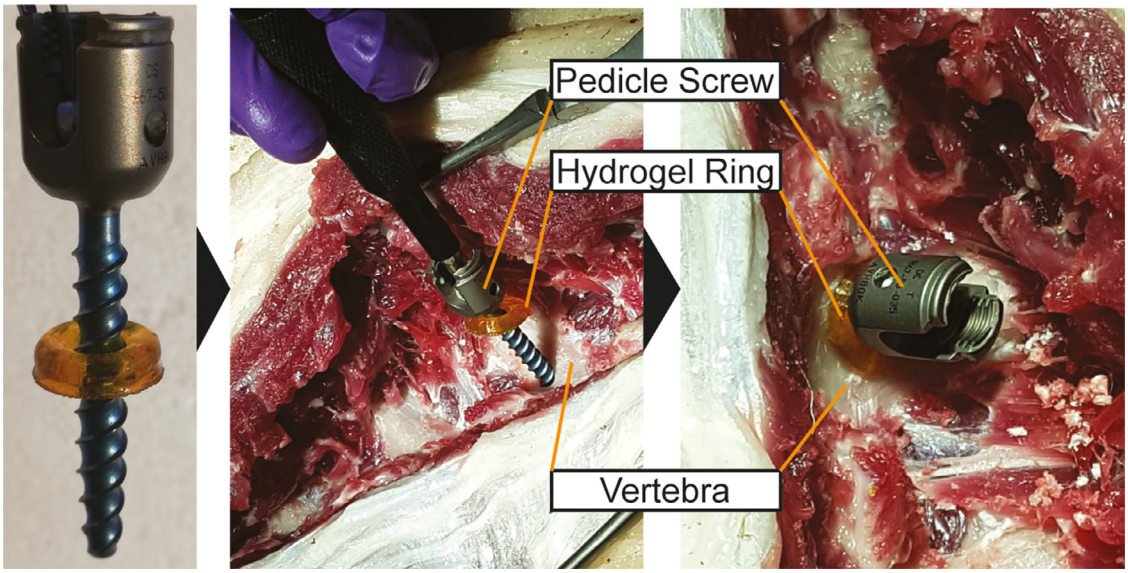


**Fig. 8.** *Ex vivo* implantability of ring-shaped hydrogel. Hydrogel rings were mounted on a 5*40 mm polyaxial pedicle screw (left). Hydrogel rings being implanted in a sheep spinal column (center). Fully inserted pedicle screw and hydrogel ring. The hydrogel ring radially expands and adapts is shape to the bone surface upon tightening of the screw (right).

to increased cell proliferation [66]. Moreover, RB deficiency has been associated with DNA and protein oxidative damage in liver cells, inhibiting cell mitosis [67]. Furthermore, the effect of glycerol and sodium bicarbonate on cell metabolism was investigated, as both were used during drug crystallization. As shown in Figure 6A, the presence of glycerol inside the hydrogels did not affect cell metabolism.

Cell viability was assessed using a Live-Dead assay. MSCs and NIH3T3 fibroblasts were seeded in a well plate and cultured in presence of hydrogels. Hydrogel compositions tested contained increasing concentrations of oB-CD with and without glycerol. No significant differences regarding cell viability were observed in NIH3T3 fibroblasts (Fig. 6B-i and Fig. S6) exposed to different concentrations of oB-CD or the presence of glycerol. In the case of MSCs, significant differences in cell viability were observed when compared to control monolayers exposed to culture medium only (Fig. 6B-ii and Fig. S6).

Next, we evaluated the cytocompatibility of hydrogels loaded with bupivacaine HCl and bupivacaine crystals (Fig. 7). NIH3T3 fibroblasts and MSCs were seeded in well plates and cultured for 24 hours in the presence of hydrogels. Exposing cells to hydrogels containing bupivacaine HCl and bupivacaine crystals caused a significant decrease in viability compared to controls. Hydrogels loaded with crystallized bupivacaine performed significantly better than hydrogels loaded with bupivacaine HCl, when culturing NIH3T3 fibroblasts for 24 hours (Fig. 7B and 7C). To understand whether this effect was due to slower release of bupivacaine from the hydrogels, or to neutralization of acidic bupivacaine following crystal formation, a Live/Dead assay was performed. NIH3T3 fibroblasts and MSCs were cultured in growth medium supplemented with i) bupivacaine HCl (1 mM in DMSO); ii) bupivacaine crystals (1 mM in DMSO and iii) the equivalent volume of DMSO used for culture i) and ii) for 24 hours (Fig. 7D-i+ii and Fig. S7). After 24 hours, the decrease in cell viability was most extensive in monolayers exposed to bupivacaine HCl dissolved in DMSO, followed by bupivacaine crystals (dissolved in DMSO) and DMSO only. This indicates that cell death induced by bupivacaine HCl is mainly due to the acidic pH. Cells were then further cultured in fresh medium for 48 hours, after which both MSCs and fibroblasts showed recovery following exposure to bupivacaine crystals. In the case of bupivacaine HCl, fibroblasts recovered better than MSCs. Overall, these results show that bupivacaine crystallization enable a sustained release with moderately decreased initial burst and improved cytocompatibility when compared to bupivacaine HCl. These properties might reduce the known myotoxic effects of bupivacaine.[68]

### 3.7. Ex vivo *implantation*

To qualitatively assess the suitability of GTA/oB-CD hydrogels for use in instrumented spinal surgery, bupivacaine-loaded hydrogel rings were co-implanted with polyaxial pedicle screws in fresh cadaveric sheep. The ring-shaped hydrogels were resistant to the forces encountered during implantation, as 19 out of 20 hydrogel rings could be implanted successfully and without any macroscopic sign of damage (*e.g.,* cracks, discoloration, tears) (Fig. 8). The design and composition of the hydrogel ring did not interfere with surgical workflow or finding the optimal screw trajectory. Due to its elasticity, the hydrogel could adapt its shape to the surgical environment. Following overtightening of screws, the rings displayed further radial expansion to accommodate the polyaxial screw head. It should be noted that none of the sheep displayed signs of spinal disease. The presence of anatomical malformations, such as scoliosis or fracture in the human patient, might complicate implantation of the screw and subsequently the hydrogel rings.

## 4. Conclusions

In summary, our study demonstrates that a GTA/oB-CD photo-crosslinked hydrogel could be a very promising system for the sustained delivery of bupivacaine for pain relief following instrumented spinal surgery. The combination of the riboflavin-mediated photo-crosslinking with the simultaneous Schiff base formation and guest-host interactions provided a tunable hydrogel displaying self-healing properties, capable of withstanding co-implantation with pedicle screws and providing sustained release for 72 hours. The GTA/oB-CD hydrogel containing *in situ* crystallized bupivacaine is cytocompatible and following release, the hydrogel is susceptible to enzymatic degradation. The moderate decrease in burst release and use of crystallized bupivacaine led to decreased cytotoxicity compared to bupivacaine HCl. This novel photo-crosslinked gelatin-based hydrogel has the potential to reduce opioid consumption fol-

lowing spinal surgery, and provide localized, sustained release of analgesics. In future, the use of this hydrogel formulation can be extended towards other implantation sites and/ or encapsulated drugs.

## Data availability

The raw data required to reproduce these findings are available upon request. Requests can be sent to the corresponding author.

## Declaration of Competing Interest

SP, JS, BO, and JJV are inventors of (U.S.) patent WO2020249695A1 covering hydrogel for *in vivo* release of medication. JS, FT, SP, BO and JJV are employed by and own stock in SentryX B.V. TV and JM report no conflicts of interest.

## Acknowledgments

The authors would like to thank Marko Mihajlovic for help with NMR experiments, Mies van Steenbergen for support and advice in mechanical testing, drug loading and quantification of release, Mattie van Rijen for general support during various stages of this study.

This study was supported by SentryX B.V., Woudenbergseweg 41, 3711AA Austerlitz, Netherlands.

## Supplementary materials

Supplementary material associated with this article can be found, in the online version, at doi:10.1016/j.actbio.2022.05.007.

## References

[1] H.J. Gerbershagen, S. Aduckathil, A.J.M. van Wijck, L.M. Peelen, C.J. Kalkman, W. Meissner, Pain intensity on the first day after surgery: a prospective cohort study comparing 179 surgical procedures, Anesthesiology 118 (2013) 934–944, doi:10.1097/ALN.0b013e31828866b3.

[2] M. Polanco-García, J. García-Lopez, N. Fàbregas, W. Meissner, M.M. Puig, PAIN-OUT-Spain consortium, postoperative pain management in Spanish hospitals: a cohort study using the PAIN-OUT registry, J. Pain. 18 (2017) 1237–1252, doi:10.1016/j.jpain.2017.05.006.

[3] E.R. Kessler, M. Shah, S.K. Gruschkus, A. Raju, Cost and quality implications of opioid-based postsurgical pain control using administrative claims data from a large health system: opioid-related adverse events and their impact on clinical and economic outcomes, Pharmacotherapy 33 (2013) 383–391, doi:10.1002/phar.1223.

[4] J.F. Barletta, Clinical and economic burden of opioid use for postsurgical pain: focus on ventilatory impairment and ileus, Pharmacotherapy 32 (2012) 12S-8S, doi:10.1002/j.1875-9114.2012.01178.x.

[5] T.J. Cicero, M.S. Ellis, Z.A. Kasper, Psychoactive substance use prior to the development of iatrogenic opioid abuse: a descriptive analysis of treatment-seeking opioid abusers, Addict. Behav. 65 (2017) 242–244, doi:10.1016/j.addbeh.2016.08.024.

[6] B.K. Madras, The surge of opioid use, addiction, and overdoses: responsibility and response of the US Health care system, JAMA Psychiatry 74 (2017) 441–442, doi:10.1001/jamapsychiatry.2017.0163.

[7] G.P. Joshi, B.O. Ogunnaike, Consequences of inadequate postoperative pain relief and chronic persistent postoperative pain, Anesthesiol. Clin. North America. 23 (2005) 21–36, doi:10.1016/j.atc.2004.11.013.

[8] T.J. Gan, Poorly controlled postoperative pain: prevalence, consequences, and prevention, J. Pain Res. 10 (2017) 2287–2298, doi:10.2147/JPR.S144066.

[9] H.A. McLure, A.P. Rubin, Review of local anaesthetic agents, Minerva Anestesiol (2005) 59–74.

[10] C.M. Santamaria, A. Woodruff, R. Yang, D.S. Kohane, Drug delivery systems for prolonged duration local anesthesia, Mater. Today (Kidlington). 20 (2017) 22–31, doi:10.1016/j.mattod.2016.11.019.

[11] M.A. Holgado, J.L. Arias, M.J. Cózar, J. Alvarez-Fuentes, A.M. Gañán-Calvo, M. Fernández-Arévalo, Synthesis of lidocaine-loaded PLGA microparticles by flow focusing, Int. J. Pharm. 358 (2008) 27–35, doi:10.1016/j.ijpharm.2008.02.012.

[12] R. Ohri, J.C.-F. Wang, P.D. Blaskovich, L.N. Pham, D.S. Costa, G.A. Nichols, W.P. Hildebrand, N.L. Scarborough, C.J. Herman, G.R. Strichartz, Inhibition by local bupivacaine-releasing microspheres of acute postoperative pain from hairy skin incision, Anesth. Analg. 117 (2013) 717–730, doi:10.1213/ANE.0b013e3182a00851.

[13] E.R. Viscusi, R. Sinatra, E. Onel, S.L. Ramamoorthy, The safety of liposome bupivacaine, a novel local analgesic formulation, Clin. J. Pain. 1 (2013), doi:10.1097/AJP.0b013e318288e1f6.

[14] J. Boogaerts, A. Declercq, N. Lafont, H. Benameur, E.M. Akodad, J.-C. Dupont, F.J. Legros, Toxicity of bupivacaine encapsulated into liposomes and injected intravenously, Anesth. Analg. 76 (1993) 553–555, doi:10.1213/00000539-199303000-00018.

[15] E. Viscusi, H. Minkowitz, P. Winkle, S. Ramamoorthy, J. Hu, N. Singla, HTX-011 reduced pain intensity and opioid consumption versus bupivacaine HCl in herniorrhaphy: results from the phase 3 EPOCH 2 study, Hernia (2019), doi:10.1007/s10029-019-02023-6.

[16] S.L. Cusack, H.S. Minkowitz, M. Kuss, M. Jaros, L. Hemsen, A randomized, multicenter, pilot study comparing the efficacy and safety of a bupivacaine-collagen implant (XaraColl(®)) with the ON-Q PainBuster(®) Post-op Pain Relief System following open gynecological surgery, J. Pain Res. 5 (2012) 453–461, doi:10.2147/JPR.S37310.

[17] J.B. McAlvin, R.F. Padera, S.A. Shankarappa, G. Reznor, A.H. Kwon, H.H. Chiang, J. Yang, D.S. Kohane, Multivesicular liposomal bupivacaine at the sciatic nerve, Biomaterials 35 (2014) 4557–4564, doi:10.1016/j.biomaterials.2014.02.015.

[18] M. Golf, S.E. Daniels, E. Onel, A phase 3, randomized, placebo-controlled trial of DepoFoam® bupivacaine (extended-release bupivacaine local analgesic) in bunionectomy, Adv. Ther. 28 (2011) 776–788, doi:10.1007/s12325-011-0052-y.

[19] A.N. Grieff, G.M. Ghobrial, J. Jallo, Use of liposomal bupivacaine in the postoperative management of posterior spinal decompression, J. Neurosurg. Spine. 25 (2016) 88–93, doi:10.3171/2015.11.SPINE15957.

[20] R. Padera, E. Bellas, J.Y. Tse, D. Hao, D.S. Kohane, Local myotoxicity from sustained release of bupivacaine from microparticles, Anesthesiology 108 (2008) 921–928, doi:10.1097/ALN.0b013e31816c8a48.

[21] D.S. Kohane, M. Lipp, R.C. Kinney, D.C. Anthony, D.N. Louis, N. Lotan, R. Langer, Biocompatibility of lipid-protein-sugar particles containing bupivacaine in the epineurium, J. Biomed. Mater. Res. 59 (2002) 450–459, doi:10.1002/jbm.1261.

[22] T.R. Hoare, D.S. Kohane, Hydrogels in drug delivery: progress and challenges, Polymer (Guildf) 49 (2008) 1993–2007, doi:10.1016/j.polymer.2008.01.027.

[23] K.R. Bagshaw, C.L. Hanenbaum, E.J. Carbone, K.W.H. Lo, C.T. Laurencin, J. Walker, L.S. Nair, Pain management via local anesthetics and responsive hydrogels, Ther. Deliv. 6 (2015) 165–176, doi:10.4155/tde.14.95.

[24] T.T. Hoang Thi, Y. Lee, S.B. Ryu, H.-J. Sung, K.D. Park, Oxidized cyclodextrin-functionalized injectable gelatin hydrogels as a new platform for tissue-adhesive hydrophobic drug delivery, RSC Adv 7 (2017) 34053–34062, doi:10.1039/C7RA04137C.

[25] M. Foox, M. Zilberman, Drug delivery from gelatin-based systems, Expert Opin. Drug Deliv. 12 (2015) 1547–1563, doi:10.1517/17425247.2015.1037272.

[26] S. Young, M. Wong, Y. Tabata, A.G. Mikos, Gelatin as a delivery vehicle for the controlled release of bioactive molecules, J. Control. Release. 109 (2005) 256–274, doi:10.1016/j.jconrel.2005.09.023.

[27] M. Zhu, Y. Wang, G. Ferracci, J. Zheng, N.J. Cho, B.H. Lee, Gelatin methacryloyl and its hydrogels with an exceptional degree of controllability and batch-to-batch consistency, Sci. Rep. (2019), doi:10.1038/s41598-019-42186-x.

[28] S. Piluso, D. Flores Gomez, I. Dokter, L. Moreira Texeira, Y. Li, J. Leijten, R. van Weeren, T. Vermonden, M. Karperien, J. Malda, Rapid and cytocompatible cell-laden silk hydrogel formation via riboflavin-mediated crosslinking, J. Mater. Chem. B. (2020), doi:10.1039/d0tb01731k.

[29] M.N. Roy, S. Saha, M. Kundu, B.C. Saha, S. Barman, Exploration of inclusion complexes of neurotransmitters with $\beta$-cyclodextrin by physicochemical techniques, Chem. Phys. Lett. 655–656 (2016) 43–50, doi:10.1016/j.cplett.2016.05.031.

[30] T.T. Hoang Thi, Y. Lee, S.B. Ryu, H.-J. Sung, K.D. Park, Oxidized cyclodextrin-functionalized injectable gelatin hydrogels as a new platform for tissue-adhesive hydrophobic drug delivery, RSC Adv 7 (2017) 34053–34062, doi:10.1039/C7RA04137C.

[31] Q. Feng, K. Wei, S. Lin, Z. Xu, Y. Sun, P. Shi, G. Li, L. Bian, Mechanically resilient, injectable, and bioadhesive supramolecular gelatin hydrogels crosslinked by weak host-guest interactions assist cell infiltration and in situ tissue regeneration, Biomaterials 101 (2016) 217–228, doi:10.1016/j.biomaterials.2016.05.043.

[32] B. Gidwani, A. Vyas, A comprehensive review on cyclodextrin-based carriers for delivery of chemotherapeutic cytotoxic anticancer drugs, Biomed Res. Int. 2015 (2015) 198268, doi:10.1155/2015/198268.

[33] M.E. Davis, M.E. Brewster, Cyclodextrin-based pharmaceutics: past, present and future, Nat. Rev. Drug Discov. (2004), doi:10.1038/nrd1576.

[34] C.M.S. Cereda, G.R. Tofoli, L.G. Maturana, A. Pierucci, L.A.S. Nunes, M. Franz-Montan, A.L.R. de Oliveira, S. Arana, D.R. de Araujo, E. de Paula, Local neurotoxicity and myotoxicity evaluation of cyclodextrin complexes of bupivacaine and ropivacaine, Anesth. Analg. 115 (2012) 1234–1241, doi:10.1213/ANE.0b013e318266f3d9.

[35] J.-Y. Lai, Biocompatibility of chemically cross-linked gelatin hydrogels for ophthalmic use, J. Mater. Sci. Mater. Med. 21 (2010) 1899–1911, doi:10.1007/s10856-010-4035-3.

[36] Sigma-Aldrich, Gelatin Product Information, 3, 2020 https://www.sigmaaldrich.com/content/dam/sigma-aldrich/docs/Sigma/Product_Information_Sheet/2/g9382pis.pdf (accessed November 17, 2020).

[37] I.D. Kuntz, F.P. Gasparro, M.D. Johnston, R.P. Taylor, Molecular interactions and the benesi-hildebrand equation, J. Am. Chem. Soc. (1968), doi:10.1021/ja01020a004.

[38] K. Sarkar, B.K. Barman, M. Nath Roy, Study to explore inclusion complexes of A- and B-cyclodextrin molecules with 3-octyl-1-methylimidazolium bromide

with the manifestation of hydrophobic and hydrophilic interactions, Chem. Phys. Lett. (2018), doi:10.1016/j.cplett.2018.07.019.
[39] N. Lohmann, L. Schirmer, P. Atallah, E. Wandel, R.A. Ferrer, C. Werner, J.C. Simon, S. Franz, U. Freudenberg, Glycosaminoglycan-based hydrogels capture inflammatory chemokines and rescue defective wound healing in mice, Sci. Transl. Med. 9 (2017), doi:10.1126/scitranslmed.aai9044.
[40] O. Hasturk, K.E. Jordan, J. Choi, D.L. Kaplan, Enzymatically crosslinked silk and silk-gelatin hydrogels with tunable gelation kinetics, mechanical properties and bioactivity for cell culture and encapsulation, Biomaterials 232 (2020) 119720, doi:10.1016/j.biomaterials.2019.119720.
[41] Worthington CorporationCollagenase product information, 2021 https://worthington-biochem.com/CLS/default.html accessed November 3, 2021.
[42] K. Siddareddy, M.A.U. Reddy, B. Suresh, J. Sreeramulu, Development and validation of analytical method for simultaneous estimation of bupivacaine and meloxicam in human plasma using UPLC-MS/MS, Pharm. Methods (2017), doi:10.5530/phm.2018.1.2.
[43] M.S. Ågren, C.J. Taplin, J.F. Woessner, W.H. Eaglstein, P.M. Mertz, Collagenase in wound healing: Effect of wound age and type, J. Invest. Dermatol. (1992), doi:10.1111/1523-1747.ep12614202.
[44] M.S. ÅGREN, Gelatinase activity during wound healing, Br. J. Dermatol. (1994), doi:10.1111/j.1365-2133.1994.tb04974.x.
[45] X. Zhao, Q. Lang, L. Yildirimer, Z.Y. Lin, W. Cui, N. Annabi, K.W. Ng, M.R. Dokmeci, A.M. Ghaemmaghami, A. Khademhosseini, Photocrosslinkable gelatin hydrogel for epidermal tissue engineering, Adv. Healthc. Mater. 5 (2016) 108–118, doi:10.1002/adhm.201500005.
[46] S.A. Madison, J.O. Carnali, pH Optimization of amidation via carbodiimides, Ind. Eng. Chem. Res. 52 (2013) 13547–13555, doi:10.1021/ie401724m.
[47] M.R. Lewis, J.Y. Kao, A.-L.J. Anderson, J.E. Shively, A. Raubitschek, An improved method for conjugating monoclonal antibodies with n -hydroxysulfosuccinimidyl DOTA, Bioconjug. Chem. 12 (2001) 320–324, doi:10.1021/bc0000886.
[48] R.W. Redmond, I.E. Kochevar, Medical applications of rose bengal- and riboflavin-photosensitized protein crosslinking, Photochem. Photobiol. 95 (2019) 1097–1115, doi:10.1111/php.13126.
[49] P. Mura, Analytical techniques for characterization of cyclodextrin complexes in aqueous solution: a review, J. Pharm. Biomed. Anal. 101 (2014) 238–250, doi:10.1016/j.jpba.2014.02.022.
[50] C. Moraes, P. Abrami, E. Depaula, A. Braga, L. Fraceto, Study of the interaction between S(−) bupivacaine and 2-hydroxypropyl-$\beta$-cyclodextrin, Int. J. Pharm. 331 (2007) 99–106, doi:10.1016/j.ijpharm.2006.09.054.
[51] M. Jug, N. Mennini, F. Melani, F. Maestrelli, P. Mura, Phase solubility, 1H NMR and molecular modelling studies of bupivacaine hydrochloride complexation with different cyclodextrin derivates, Chem. Phys. Lett. 500 (2010) 347–354, doi:10.1016/j.cplett.2010.10.046.
[52] N.A. Peppas, P. Bures, W. Leobandung, H. Ichikawa, Hydrogels in pharmaceutical formulations, Eur. J. Pharm. Biopharm. 50 (2000) 27–46, doi:10.1016/s0939-6411(00)00090-4.
[53] H. Park, X. Guo, J.S. Temenoff, Y. Tabata, A.I. Caplan, F.K. Kasper, A.G. Mikos, Effect of swelling ratio of injectable hydrogel composites on chondrogenic differentiation of encapsulated rabbit marrow mesenchymal stem cells in vitro, Biomacromolecules 10 (2009) 541–546, doi:10.1021/bm801197m.
[54] K. Yue, G. Trujillo-de Santiago, M.M. Alvarez, A. Tamayol, N. Annabi, A. Khademhosseini, Synthesis, properties, and biomedical applications of gelatin methacryloyl (GelMA) hydrogels, Biomaterials (2015), doi:10.1016/j.biomaterials.2015.08.045.
[55] Y. Wu, Y. Xiang, J. Fang, X. Li, Z. Lin, G. Dai, J. Yin, P. Wei, D. Zhang, The influence of the stiffness of GelMA substrate on the outgrowth of PC12 cells, Biosci. Rep. 39 (2019), doi:10.1042/BSR20181748.
[56] H. Sun, L. Mei, C. Song, X. Cui, P. Wang, The in vivo degradation, absorption and excretion of PCL-based implant, Biomaterials 27 (2006) 1735–1740, doi:10.1016/j.biomaterials.2005.09.019.
[57] A.C.R. Grayson, G. Voskerician, A. Lynn, J.M. Anderson, M.J. Cima, R. Langer, Differential degradation rates in vivo and in vitro of biocompatible poly(lactic acid) and poly(glycolic acid) homo- and co-polymers for a polymeric drug-delivery microchip, J. Biomater. Sci. Polym. Ed. 15 (2004) 1281–1304, doi:10.1163/1568562041959991.
[58] Sigma Aldrich, Collagenase from C. histolyticum Product Information, (n.d.) 1–3. https://www.sigmaaldrich.com/content/dam/sigma-aldrich/docs/Sigma/Datasheet/3/c9891dat.pdf (accessed December 18, 2020).
[59] Q. Xing, K. Yates, C. Vogt, Z. Qian, M.C. Frost, F. Zhao, Increasing mechanical strength of gelatin hydrogels by divalent metal ion removal, Sci. Rep. (2014), doi:10.1038/srep04706.
[60] S. Piluso, A. Lendlein, A.T. Neffe, Enzymatic action as switch of bulk to surface degradation of clicked gelatin-based networks, Polym. Adv. Technol. 28 (2017) 1318–1324, doi:10.1002/pat.3962.
[61] H.P. Erickson, Size and shape of protein molecules at the nanometer level determined by sedimentation, gel filtration, and electron microscopy, Biol. Proced. Online. 11 (2009) 32–51, doi:10.1007/s12575-009-9008-x.
[62] T. Ci, Y. Shen, S. Cui, R. Liu, L. Yu, J. Ding, Achieving high drug loading and sustained release of hydrophobic drugs in hydrogels through in situ crystallization, Macromol. Biosci. (2017), doi:10.1002/mabi.201600299.
[63] S. McDonald, A.A. Faibushevich, S. Garnick, K. Mclaughlin, C. Lunte, M. S., F. A.A., G. S., M. K., L. C., Determination of local tissue concentrations of bupivacaine released from biodegradable microspheres and the effect of vasoactive compounds on bupivacaine tissue clearance studied by microdialysis sampling, Pharm. Res. 19 (2002) 1745–1752, doi:10.1023/A:1020725917197.
[64] H.S. Feldman, P. Hartvig, L. Wiklund, A.M. Doucette, G. Antoni, A. Gee, J. Ulin, B. Langstrom, Regional distribution of 11C-labeled lidocaine, bupivacaine, and ropivacaine in the heart, lungs, and skeletal muscle of pigs studied with positron emission tomography, Biopharm. Drug Dispos. 18 (1997) 151–164 https://doi.org/10.1002/(sici)1099-081x(199703)18:2<151::aid-bdd8>3.0.co;2-h.
[65] A.I. Caplan, Mesenchymal stem cells, J. Orthop. Res. 9 (1991) 641–650, doi:10.1002/jor.1100090504.
[66] E. Nakano, S. Mushtaq, P.R. Heath, E.S. Lee, J.P. Bury, S.A. Riley, H.J. Powers, B.M. Corfe, Riboflavin depletion impairs cell proliferation in adult human duodenum: Identification of potential effectors, Dig. Dis. Sci. (2011), doi:10.1007/s10620-010-1374-3.
[67] K.C. Manthey, R. Rodriguez-Melendez, J.T. Hoi, J. Zempleni, Riboflavin deficiency causes protein and DNA damage in HepG2 cells, triggering arrest in G1 phase of the cell cycle, J. Nutr. Biochem. 17 (2006) 250–256, doi:10.1016/j.jnutbio.2005.05.004.
[68] J.G. Steverink, S. Piluso, J. Malda, J.-J. Verlaan, Comparison of in vitro and in vivo Toxicity of Bupivacaine in Musculoskeletal applications, Front. Pain Res 2 (2021), doi:10.3389/fpain.2021.723883.